# NATIONAL ADVISORY COMMITTEE FOR AERONAUTICS

**TECHNICAL NOTE 2592**

# ORIENTATION OF ORIFICES ON BODIES OF REVOLUTION FOR DETERMINATION OF STREAM STATIC PRESSURE AT SUPERSONIC SPEEDS

By Morton Cooper and Clyde V. Hamilton

Langley Aeronautical Laboratory
Langley Field, Va.

Washington

January 1952

NATIONAL ADVISORY COMMITTEE FOR AERONAUTICS

TECHNICAL NOTE 2592

# ORIENTATION OF ORIFICES ON BODIES OF REVOLUTION FOR DETERMINATION OF STREAM STATIC PRESSURE AT SUPERSONIC SPEEDS

By Morton Cooper and Clyde V. Hamilton

## SUMMARY

Experimental data obtained in the Langley 4- by 4-foot supersonic tunnel for a parabolic body of revolution of large fineness ratio at a Mach number of 1.59 and a Reynolds number of $3.6 \times 10^6$ have been analyzed to locate positions at which static-pressure orifices will indicate a constant static pressure (stream static or otherwise) independent of the pitch-yaw attitude of the body. The results show that by locating two orifices at symmetrical radial positions with respect to the angle-of-attack plane and by using a single pressure given by the average of the two orifice readings, appreciable pitch-yaw ranges can be obtained while a constant static pressure is maintained. The proper radial positions of the orifices vary with the axial location. At the front of the body tested, the proper radial positions are $\pm 67^\circ$ measured from the bottom of the body; at 1/3 of the body length, the locations are $\pm 52^\circ$; and at the maximum diameter, the locations are $\pm 37.5^\circ$. For this Mach number and at these stations, the maximum angles of attack obtainable within a static-pressure error of $1\frac{3}{4}$ percent were $10^\circ$, $20^\circ$, and $16^\circ$, respectively. These angle-of-attack limits were unchanged by yaw provided the yaw angles were less than $\pm 5^\circ$, $\pm 8^\circ$, and $\pm 5^\circ$, respectively.

## INTRODUCTION

The accurate determination of the free-stream static pressure in airspeed-measurement systems invariably poses a difficult problem. In general, static-pressure orifices, unlike total-pressure orifices, are extremely sensitive to air-stream direction (reference 1) so that an accurate measurement of the static pressure without previous knowledge of the flow direction is exceedingly difficult. This problem has always been present at subsonic speeds and has been recently reemphasized at supersonic speeds in connection with aircraft and missile flight.

Various techniques have been considered for determining the free-stream static pressures. The pitot-static tube is the most versatile since it can, in general, be used for both subsonic and supersonic speeds. Limitation to incidence angles of the order of $5^{\circ}$ because of static-pressure errors is the principal drawback of the conventional pitot-static tube. Free-floating mass-balanced tubes are, of course, ideal solutions aerodynamically since, at all speeds, they eliminate pressure errors due to the flow misalinement and, in addition, provide a direct means for obtaining the flow angles. Mechanically, however, this type of instrument is, at present, somewhat unwieldy and complicated for many applications. For use at supersonic speeds, the cone (see reference 2, for example) also provides a means for determining the free-stream pressures (Mach number) and flow angles.

The present paper further considers some of the problems of determining the free-stream static pressure from bodies of revolution for use in airspeed systems at supersonic speeds. By a simple application of slender-body theory, points are located on a body where only very small pressure changes occur with incidence. These points may then be considered as the proper locations for static-pressure orifices. Experimental data obtained during a detailed pressure-distribution investigation of a parabolic body of revolution at a Mach number of 1.59 and a Reynolds number of $3.6 \times 10^{6}$ are then analyzed; the trends predicted are substantiated and slight empirical modifications to the theoretical locations are indicated. The results of this analysis may be applied for the location of static-pressure vents on some missile and aircraft configurations or more generally in the design of static-pressure probes.

## SYMBOLS

Free-stream conditions:

| | |
|---|---|
| $\rho$ | mass density of air |
| $V$ | airspeed |
| $a$ | speed of sound in air |
| $M$ | Mach number $(V/a)$ |
| $q$ | dynamic pressure $\left(\frac{1}{2}\rho V^2\right)$ |
| $p$ | static pressure |

Body geometry:

| | |
|---|---|
| $\alpha$ | angle of attack of axis of body, degrees |
| $\psi$ | angle of yaw of axis of body, degrees |
| $\epsilon$ | incidence angle, angle between axis of body and relative wind; radians in equations, degrees in figures and table |
| $\epsilon_{max}$ | maximum incidence angle, degrees |
| $\phi$ | radial angle of body measured from plane of incidence angle ($0^\circ$ on side air-stream impinges; positive counterclockwise when viewed from rear, see fig. 1) |
| $\phi_0$ | radial angle of body measured from plane of angle of attack ($0^\circ$ on side air-stream impinges; positive counterclockwise when viewed from rear; equal to $\phi$ when yaw is absent) |
| x | distance along axis of body measured from origin at nose |
| $x_{r_{max}}$ | distance along axis from nose to station of maximum thickness |
| r | radius of body at a given axial station |
| $r_{max}$ | radius of body at maximum thickness |
| L | length of body |

Pressure data:

| | |
|---|---|
| $p_l$ | local static pressure |
| P | pressure coefficient $\left(\frac{p_l - p}{q}\right)$ |
| $\overline{p_l}$ | local static pressure on surface of body in axially symmetric flow |
| $\overline{P}$ | pressure coefficient on surface of body in axially symmetric flow |
| $\Delta P$ | incremental pressure coefficient due to incidence angle (see equation (1)) |

## APPARATUS

Tunnel.- The Langley 4- by 4-foot supersonic tunnel is a rectangular, closed-throat, single-return wind tunnel designed for a nominal Mach number range from 1.2 to 2.2. The test-section Mach number is varied by deflecting horizontal flexible walls against a series of fixed interchangeable templets which have been designed to produce uniform flow in the test section. For the present investigation, the nozzle walls were set for a test-section Mach number of 1.59. For this Mach number, the test section has a width of 4.5 feet and a height of 4.4 feet. Detailed calibrations of the test section have shown that the general flow properties have a relatively high degree of uniformity. (See table I of reference 2.)

Model.- The test model, shown in figure 1, was a parabolic body of revolution constructed of steel. The rear part of the model was cut off at a station 42.05 inches from the apex; so that the over-all fineness ratio was reduced from 15 to 12.2. The experimental data presented in this paper were obtained from a total of 24 static-pressure orifices 0.020-inch in diameter; four orifices were spaced 90° apart radially at each of the following longitudinal (x/L) stations: 0.024, 0.167, 0.333, 0.476, 0.618, and 0.714.

Installation.- The model was sting-supported in the tunnel (fig. 2) and the incidence was varied in the horizontal plane. In order to define accurately the radial pressure distributions at a given axial station, the model was rotated in fixed increments of approximately 15° in order to provide a more detailed orifice coverage.

## TESTS AND CORRECTIONS

Tests.- The data were obtained for a range of incidence angles from 0° to 36° at a Mach number of 1.59 and a Reynolds number of $3.60 \times 10^6$ based on body length. The tunnel stagnation conditions were: pressure, 0.25 atmosphere; temperature, 110° F; and dew point, -35° F. For these test conditions, the calibration data of the test section indicate that the effects of condensation on the flow over the model are probably extremely small.

Corrections.- Since the magnitudes of the flow angle, Mach number, and pressure gradients are small in the vicinity of the model, no corrections for these effects have, in general, been applied to the data. A specific illustration of the negligible influence of flow angularity on the incidence angles is presented in reference 2. Angular corrections due to aerodynamic loads and model "droop" (due to the weight of the model) have been applied as discussed in reference 2. The maximum

magnitude of these combined corrections was 0.28°. For these tests (unlike those reported in reference 2), a special rig was installed so that the model could be alined with the air stream for the test at zero incidence; consequently, no corrections were necessary for this condition.

## RESULTS AND ANALYSIS

Basic considerations.- In order to investigate the flow over an inclined body and to locate a point where the pressure is independent of angle of incidence, the body is treated as a slender body and the flow over it is determined by a linearized approach. The pressure coefficient at any point on the surface of an inclined body of revolution is given by (reference 3):

$$P = \bar{P} + \Delta P \epsilon \cos \phi + (1 - 4 \sin^2 \phi)\epsilon^2 \tag{1}$$

where $\bar{P}$ is the pressure coefficient on the surface of the body when the body axis is alined with the air stream (references 4 and 5), and $\Delta P$ is an incremental pressure coefficient due to incidence (references 4 and 6). For slender bodies, $\Delta P$ has the value $4 \frac{dr}{dx}$. Equation (1) is, of course, not restricted to a cylindrical body inasmuch as the local radius may be a function of x. The succeeding analysis, however, is restricted primarily to a parabolic body of revolution only because experimental data are available for a detailed discussion of such a body. The analysis, however, applies to the conventional cylindrical static-pressure tube as a special case. If the restriction of a parabolic body is imposed, the pressure coefficient in axially symmetric supersonic flow is given by:

$$\bar{P} = \left(\frac{2r_{max}}{x_{r_{max}}}\right)^2 \left\{ \frac{3 - 9\left(\frac{x}{x_{r_{max}}} - 1\right)}{2} \sqrt{\left(\frac{x}{x_{r_{max}}}\right)^2 - (M^2 - 1)\left(\frac{r}{x_{r_{max}}}\right)^2} + \left[ 3\left(\frac{x}{x_{r_{max}}} - 1\right)^2 - 1 + \frac{3}{2}(M^2 - 1)\left(\frac{r}{x_{r_{max}}}\right)^2 \right] \cosh^{-1} \frac{x}{r\sqrt{M^2 - 1}} \right\} - \left(\frac{2r_{max}}{x_{r_{max}}}\right)^2 \left(1 - \frac{x}{x_{r_{max}}}\right)^2 \tag{2}$$

In order to establish a point on the body where the pressure is equal to the free-stream static pressure, the coefficient $P$ in equation (1) is zero by definition, and the radial position $\phi$ can be evaluated as a function of the incidence angle, the body shape, and the Mach number to satisfy such a requirement. The selection of $P$ equal to zero is convenient because the orifice would then read free-stream static pressure directly. Such a condition initially, however, imposes an unnecessarily stringent requirement because, for low incidences, the static-pressure coefficient in axially symmetric flow $\bar{P}$ is always greater than zero for the forward part of the body. The forward region, thus, would automatically be eliminated from consideration until some finite incidence angle is reached where the additional terms due to incidence (equation (1)) cancel the positive value of $\bar{P}$. In order to avoid this limitation, the requirement is established that $P$, the pressure coefficient at an angle of attack must equal the zero-incidence value $\bar{P}$; the correction to free-stream static pressure is then determined from equation (2) if a total-pressure-tube reading is available.

If $P$ is set equal to $\bar{P}$ in equation (1), the radial position $\phi$ is given as a function of incidence and body shape by:

$$\phi = \cos^{-1} \frac{-\left(\frac{1}{\epsilon}\frac{dr}{dx}\right) \pm \sqrt{\left(\frac{1}{\epsilon}\frac{dr}{dx}\right)^2 + 3}}{2} \qquad (3)$$

where the plus sign represents values on the upwind (first and fourth quadrant) side and the minus sign represents values on the downwind (second and third quadrant) side. This equation (plotted in fig. 3) shows that the radial position $\phi$, where $P = \bar{P}$, is a function solely of the parameter $\frac{1}{\epsilon}\frac{dr}{dx}$. Furthermore, if $\phi$ is to be independent of incidence, $dr/dx$ must equal zero. The theoretically ideal orifice location therefore occurs at the station of maximum diameter $\left(\frac{dr}{dx} = 0\right)$ and at a radial location of $30^\circ$ or $150^\circ$.

In order to check the validity of equation (3), experimental pressure distributions have been analyzed for six stations along the body for a range of incidence angles. The locations of these stations are shown in figure 1. A representative part of the experimental data for a station located at $\frac{x}{L} = 0.024$ is plotted in figure 4 for incidence angles up to $16.10^\circ$. Since the flow is essentially symmetrical with respect to the $0^\circ$ to $180^\circ$ axis for this station and incidence range, the horizontal scale in figure 4 represents both positive and negative values of $\phi$.

For each incidence angle $\epsilon$ and each of the six stations (various dr/dx values), the radial position $\phi$ where the pressure distribution intersected the $\epsilon = 0$ curve was read and plotted in figure 3; the individual points are presented in table I. As can be seen from the experimental-theoretical comparison of figure 3, the results reduce substantially to a single-parameter curve as predicted by theory; the experimental curve, however, shows radial positions somewhat greater than theory and gives an indication of the limits of the theory. Data for angles of incidence much greater than 20° scatter appreciably and do not appear to reduce to a single-parameter curve. Only a limited amount of experimental data exists for the branch of the theoretical curve corresponding to radial positions greater than 100°. Since the incidence angle $\epsilon$ is positive, points on this secondary branch of the curve must come primarily from regions of the body having a negative slope (stations 0.618 and 0.714). The experimental data presented correspond to such stations. (See tabel I.) For the higher angles of incidence, separation on the downwind side of the body for these stations prevents the existence of any additional points.

The most noticeable discrepancies shown in figure 3 occur for the points at a low incidence angle, namely $\epsilon = 2.00°$. These discrepancies are precision limitations on the data reduction, as can be seen from figure 4, rather than limitations on the theory. In order to determine the radial position for $P = \bar{P}$ for $\epsilon = 2.00°$ from figure 4, it is necessary to read the intersection point of two experimental curves which intersect with a small included angle. Even the slightest changes in the fairing of either of these curves suffice to move the radial points about 10° to 15° for the $\epsilon = 2.00°$ results. From the over-all comparison presented in figure 3, the proper location for an orifice at the maximum diameter appears to be at a radial position between 35° and 40°, perhaps at 37.5°.

Effects of body station on orifice location.- In order to consider the data of figure 3 more fully, three particular reference stations have been selected and the radial locations for $P = \bar{P}$ for these stations have been plotted as a function of incidence angle in figure 5. The station $\left(\frac{x}{L} = 0.614\right)$ for the theoretically ideal location also is included in this figure. Although no data are available at this station, it is sufficiently close to station 0.618 that differences in the results for the two stations would be negligible for all practical purposes. From practical considerations, two additional bracketing curves (dashed lines) representing a ±0.01 difference in pressure coefficient from the axially symmetric value have been added for each station on figure 5 to serve as sensitivity boundaries. If a point is enclosed by these boundaries, this point is assumed to indicate the static pressure. The value of 0.01 in pressure coefficient (corresponding to a static-pressure error of approximately $1\frac{3}{4}$ percent at a Mach number of 1.59) was selected because it

represents an over-all limitation on the accuracy of the experimental data. The corresponding experimental data for each curve have also been included in this figure. In general, the experimental data follow the trends of the theoretical curves in the low-incidence range (possibly up to $7^\circ$ to $10^\circ$) but diverge at higher angles, the theoretical curves being consistently low above about $10^\circ$ incidence. For these higher angles, of course, the comparison with a linearized theory is rather academic.

As was pointed out in connection with figure 3, the theoretical results predict values of the radial position which are too low. In order to consider the effects of the precision limits on the reduction of the data, some of the experimental data were replotted and refaired completely independently of the first set. The final results from the second data reduction are flagged in figure 5 and in subsequent figures. It is evident from the scatter between the flagged and unflagged symbols that the limitations on the accuracy of the reduction of the experimental data are restricted to the lower angles as previously mentioned. Although the theoretically ideal orifice location occurs at station 0.614 $\left(\frac{dr}{dx} = 0\right)$, figure 5 clearly indicates both experimentally and theoretically that reasonably high incidence angles can be obtained at the other stations without exceeding the prescribed precision limits. For example, according to the experimental data (fig. 5), an orifice located at station 0.333 and at a radial position of $52^\circ$ would indicate a pressure coefficient within 0.01 of the zero incidence value up to about $21^\circ$ incidence. This point is illustrated more clearly in figure 6 which indicates the useful incidence-angle range as a function of body station for a fixed-orifice installation.

In figure 6(a), the theoretical maximum incidence angles are plotted (solid line) as a function of body station; the corresponding fixed radial positions are shown (solid line) in figure 6(b). Theoretically, an orifice located at the position shown in figure 6(b) will indicate a pressure coefficient within 0.01 of the value at $0^\circ$ incidence up to the incidence angle specified in figure 6(a). A linearized theory has been used so that the curves are only indicative at best. Two sets of experimental data have been presented in figure 6: one set (circles) indicates the maximum value of $\epsilon$ obtained for orifices located at the theoretical radial positions and the second set (squares) corresponds to orifices located at modified radial positions. These modified positions were selected on the basis of the experimental data of figures 3 and 5. For both sets of data, the maximum incidence angles were obtained by plotting the pressure coefficient as a function of incidence angle (figs. 7 and 8) for the appropriate radial positions and by reading the intersection of the resultant curve with the sensitivity boundary. (For example, see fig. 8, station 0.333.) It is immediately apparent that on the basis of the modified radial locations (figs. 6 or 8) reasonably high incidence angles are possible, the magnitudes of which are summarized in the following table:

| Station x/L | Orifice location $\phi$ (deg) | Maximum incidence angle for assumed pressure coefficient sensitivity of 0.01 (deg) |
|---|---|---|
| 0.024 | 67 | 10 |
| .333 | 52 | 21 |
| .618 | 37.5 | 16 |

It should be noted (fig. 8) that, at station 0.333, where a maximum incidence angle of 21° is obtainable, the orifice indicates the free-stream static pressure directly, that is, $P = \overline{P} \approx 0$. Although the high values of the tabulated incidence angles are probably very close to the optimum values, slight shifts in the radial position might increase the maximum incidence angles slightly.

The comparison of the experimental and theoretical maximum incidence angles for the theoretical radial locations (fig. 6) shows these positions in a very pessimistic light since the maximum experimental values of incidence angle are too small for any practical purposes. The data of figure 7 indicate that at station 0.024 a slight increase in the sensitivity boundary increases the allowable maximum incidence angle appreciably. In the interpretation of these particular data for the theoretical orifice locations, it should be realized that an extremely critical application of theory has been made in that the maximum discrepancy tolerated between experiment and theory in the pressure increment due to incidence is only 0.01 in pressure coefficient. The data of figure 6 or 8 show that for all axial stations the permissible incidence angles at the modified radial locations are relatively high, at least 10°, so that further considerations are not restricted to the theoretical station $\left(\frac{dr}{dx} = 0\right)$ for maximum incidence.

The main problems as yet to be considered in the analysis involve the following:

(1) The effects of yaw on the static pressures since, up to the present, it has been tacitly assumed that no yaw is present.

(2) The effects of Mach number on the static-pressure readings.

Yaw effects.- The entire analysis in the preceding section has been in terms of the incidence angle which is defined as the angle between the body axis and the relative wind. In practical configurations which use a fixed-orifice position, interpretation of these results in terms of pitch and yaw is more important; hence, the incidence angle has been

geometrically separated into pitch and yaw angles. Since the incidence angles have been separated into pitch and yaw angles, the radial orifice location is indicated by $\phi_0$. The determination of the pitch and yaw attitudes from a given set of incidence data can be made by resolving the incidence angle $\epsilon$ to any pitch-yaw attitude corresponding to this incidence. (See reference 2, for example.) When this resolution was made, the incidence angle was assumed to be small so that it could be taken directly as the vector sum of the angle of attack and the angle of yaw. The results of this analysis are presented in figures 9 to 11 for the three representative stations for which experimental data have been obtained. For each station, the maximum permissible yaw boundaries are plotted as a function of angle of attack for the theoretical radial orifice locations in part (a) of figures 9 to 11; and for the modified radial locations in parts (b) and (c) of figures 9 to 11.[1] For the modified radial locations, two separate systems are considered. One system (part (b) of figs. 9 to 11) utilizes a single orifice located as specified ($\phi_0$) with respect to the angle-of-attack plane; the second system (part (c) of figs. 9 to 11) utilizes two orifices located symmetrically with respect to the angle-of-attack plane. In this second system, the two orifices are assumed to be connected to a common chamber with only the chamber pressure known. For the purpose of this analysis, the chamber pressure is assumed to be equal to the average of the pressure readings at the two individual orifices. For figures 9 to 11, the theoretical curves correspond to the theoretical radial positions of the orifices. For a given attitude to remain within the prescribed sensitivity requirements, the point must remain between the boundary curves shown.

The data of figures 9 to 11 reemphasize the superiority of the modified orifice locations and indicate an appreciable improvement as regards maximum attainable angle of attack without yaw. It is quite evident, however, that a single orifice (part (b) of figs. 9 to 11) located even at the modified radial position is quite limited with respect to yaw considerations. The regions of the curves (part (b) of figs. 9 to 11) corresponding to large yaw values are of no practical significance since they correspond to such specialized pitch-yaw combinations. The two-orifice system (part (c) of figs. 9 to 11) shows a marked improvement with respect to yaw although, as would be anticipated, no change in maximum attainable angle of attack occurs. This improvement results from the balancing of opposing trends on the individual orifices.

---

[1]Although pitch and yaw attitude have been treated as the geometric variables in the present section and in figures 9 to 11, it should be noted that the conversion to equivalant roll angle at fixed incidence can be accomplished by means of the approximate relations:

$$\text{Roll angle} = -\tan^{-1}\frac{\psi}{\alpha}$$

$$\epsilon = \sqrt{\alpha^2 + \psi^2}$$

In general, the maximum practical pitch-yaw ranges for a two-orifice system are:

| Station x/L | Orifice locations $\phi$ (deg) | Maximum angle of attack (deg) | Maximum yaw angle (deg) |
|---|---|---|---|
| 0.024 | ±67 | 10 | ±5 |
| .333 | ±52 | 20 | ±8 |
| .618 | ±37.5 | 16 | ±5 |

A slight increase in maximum angle of attack to 21° is possible for station 0.333 (fig. 10(c)) at a sacrifice in yaw-angle range.

In reality, the experimental boundary curves presented in part (c) of figures 9 to 11 were not symmetrical with respect to positive and negative yaw at the high incidence angles due to asymmetrical separation over the downwind side of the body. Since the regions of the boundary curves affected by this asymmetrical separation are outside the useful limits for the present discussion, the boundary curves were made symmetrical by taking the flow over one side of the body to be the same as over the other side.

Further improvement in both systems with regard to yaw considerations may be possible if a single counter-balanced fin is mounted on the tube and the tube is allowed one degree of freedom to rotate about its own axis so that the orifices are alined in the plane of the incidence angle. Such a scheme, however, would probably entail a separate investigation.

Mach number effects.- According to the approximate theory, the pressures due to incidence are not affected by Mach number; therefore, in the absence of additional experimental data on this model at other Mach numbers to examine the validity of this approximation, the influence of Mach number on the static pressure in axially symmetric flow only is considered. The dependence of this pressure on the Mach number (equation (2)) is shown in figure 12 in terms of the pressure coefficient and the static-pressure ratio. The effects of Mach number are small. If a total-pressure reading is available, a correction factor, obtainable from figure 12, can be applied since the Mach number is established when the surface pressure and the total pressure are known.

The effects of Mach number also enter the analysis in the assumed sensitivity of 0.01 in pressure coefficient. This value corresponds to a static-pressure error of approximately 1 percent at a Mach number of 1.2 and 4.5 percent at a Mach number of 2.5. For a fixed percentage error in static pressures, therefore, the permissible error in pressure coefficient must decrease with Mach number.

The magnitude and variation with Mach number of the pressure coefficient for zero incidence ($\bar{P}$) depends upon the slenderness of the body,

both decreasing as the body becomes more slender. This result indicates the desirability of using a conventional cylindrical pitot-static or static tube alone. For such a tube, with the static orifices sufficiently far from the nose, the pressure coefficient $\overline{P}$ is zero for all Mach numbers (subsonic and supersonic) and the ideal radial locations for a 2-orifice system are theoretically $\pm 30^{\circ}$. Some modification in the direction of $\pm 37.5^{\circ}$, however, might prove advantageous as was the case for the parabolic body.

## CONCLUDING REMARKS

Experimental data obtained in the Langley 4- by 4-foot supersonic tunnel for a parabolic body of revolution of large fineness ratio at a Mach number of 1.59 and a Reynolds number of $3.6 \times 10^6$ have been analyzed to locate positions at which static-pressure orifices indicated a constant static pressure (stream static or otherwise) independent of the pitch-yaw attitude of the body. The results show that, by locating two orifices at symmetrical radial positions with respect to the angle-of-attack plane and by using a single pressure given by the average of the two orifice readings, appreciable pitch-yaw ranges can be obtained while a constant static pressure is maintained. The proper radial positions of the orifices vary with the axial location. At the front of the body tested, the proper radial positions are $\pm 67^{\circ}$ measured from the bottom of the body; at 1/3 of the body length, the locations are $\pm 52^{\circ}$; and at the maximum diameter, the locations are $\pm 37.5^{\circ}$. For this Mach number and at these stations, the maximum angles of attack obtainable within a static-pressure error of $1\frac{3}{4}$ percent were $10^{\circ}$, $20^{\circ}$, and $16^{\circ}$, respectively. These angle-of-attack limits were unchanged by yaw provided the yaw angles were less than $\pm 5^{\circ}$, $\pm 8^{\circ}$, and $\pm 5^{\circ}$, respectively.

Langley Aeronautical Laboratory
National Advisory Committee for Aeronautics
Langley Field, Va., September 19, 1951

## REFERENCES

1. Fluid Motion Panel of the Aeronautical Research Committee and Others: Modern Developments in Fluid Dynamics. Vol. I, ch. VI, sec. 11, S. Goldstein, ed., The Clarendon Press (Oxford), 1938, pp. 248-254.

2. Cooper, Morton, and Webster, Robert A.: The Use of an Uncalibrated Cone for Determination of Flow Angles and Mach Numbers at Supersonic Speeds. NACA TN 2190, 1951.

3. Allen, H. Julian: Pressure Distribution and Some Effects of Viscosity on Slender Inclined Bodies of Revolution. NACA TN 2044, 1950.

4. Lighthill, M. J.: Supersonic Flow past Bodies of Revolution. R. & M. No. 2003, British A.R.C., 1945.

5. Lighthill, M. J.: Methods for Predicting Phenomena in the High-Speed Flow of Gases. Jour. Aero. Sci., vol. 16, no. 2, Feb. 1949, pp. 69-83.

6. Tsien, Hsue-Shen: Supersonic Flow over an Inclined Body of Revolution. Jour. Aero. Sci., vol. 5, no. 12, Oct. 1938, pp. 480-483.

TABLE I.- RADIAL POSITION FOR $P = \overline{P}$

| Station x/L | 0.024 | | 0.167 | | 0.333 | | 0.476 | | 0.618 | | 0.714 | |
|---|---|---|---|---|---|---|---|---|---|---|---|---|
| $\epsilon$ (deg) | $\frac{1}{\epsilon}\frac{dr}{dx}$ | $\phi$ (deg) | $\frac{1}{\epsilon}\frac{dr}{dx}$ | $\phi$ (deg) | $\frac{1}{\epsilon}\frac{dr}{dx}$ | $\phi$ (deg) | $\frac{1}{\epsilon}\frac{dr}{dx}$ | $\phi$ (deg) | $\frac{1}{\epsilon}\frac{dr}{dx}$ | $\phi$ (deg) | $\frac{1}{\epsilon}\frac{dr}{dx}$ | $\phi$ (deg) |
| 2.00 | 0.0642 | 83 | 0.0486 | 86 | 0.0306 | 90 | 0.0151 | 68 | -0.00045 | 56/150 | -0.0108 | 45/140 |
| 4.00 | .0316 | 75 | .0243 | 72 | .0153 | 71 | .0075 | 62 | -.0002 | 45/168 | -.0054 | 28/135 |
| 8.05 | .0161 | 66 | .0122 | 58 | .0076 | 56 | .0038 | 44 | -.0001 | 35/177 | -.0027 | 27/162 |
| 12.05 | .0106 | 60 | .0081 | 56 | .0051 | 54 | .0025 | 46 | -.0001 | 38 | -.0018 | 32 |
| 16.10 | .0080 | 58 | .0061 | 55 | .0038 | 51 | .0019 | 45 | -.0001 | 39 | -.0013 | 36 |
| 20.00 | .0064 | 56 | .0049 | 56 | .0031 | 53 | .0015 | 47 | -.0001 | 38 | -.0011 | 39 |

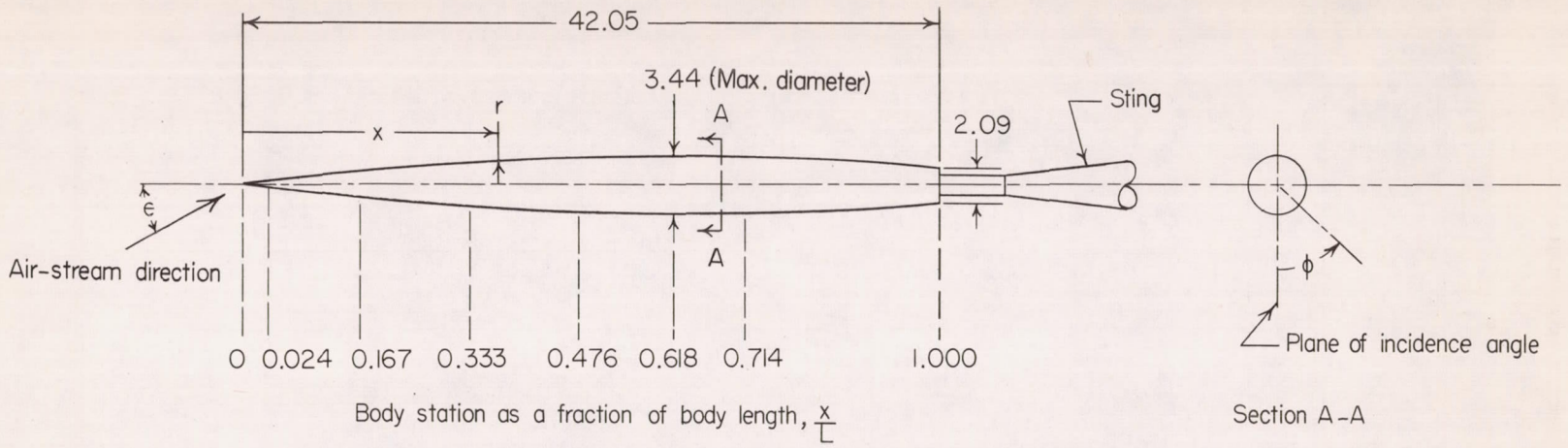


$$r = 1.722\left[\frac{2x}{25.83} - \left(\frac{x}{25.83}\right)^2\right]$$

Figure 1.- Scale drawing of test model. (All dimensions are in inches unless otherwise specified.)

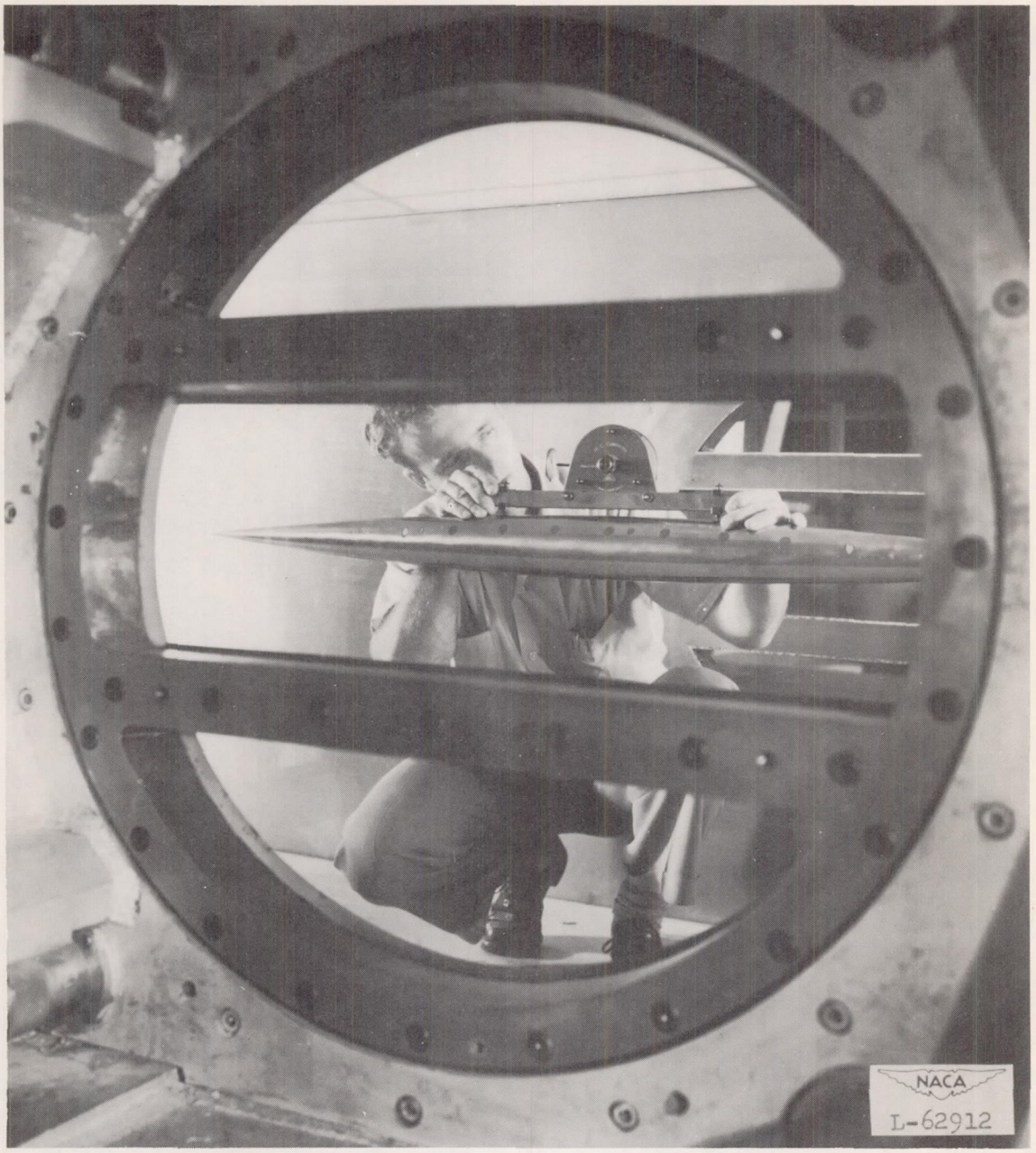


Figure 2.- Model mounted in test section of the Langley 4- by 4-foot supersonic tunnel.

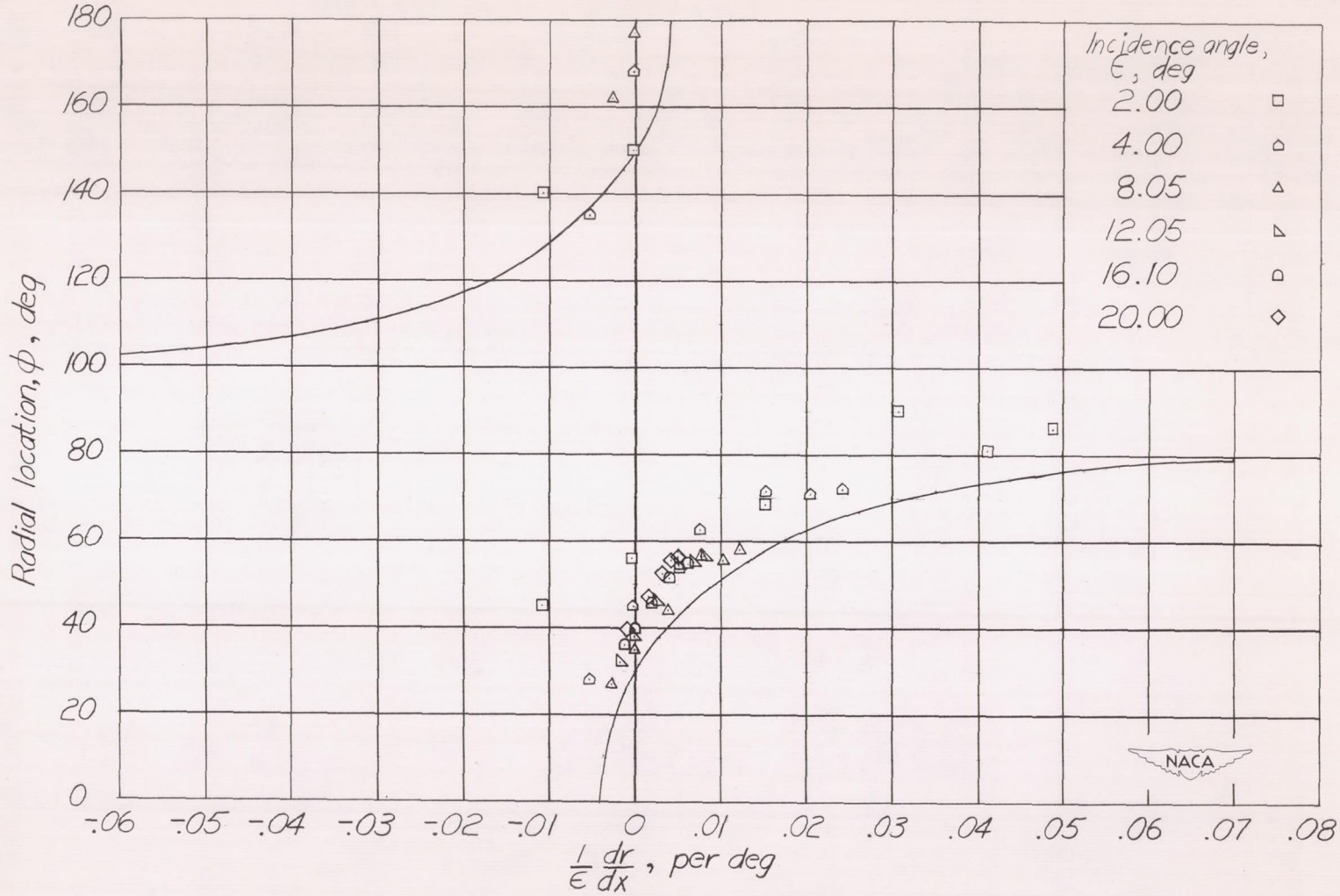


Figure 3.- Radial orifice locations for constant static pressure ($p = \bar{p}$) as a function of body slope and incidence angle for a parabolic body of revolution.

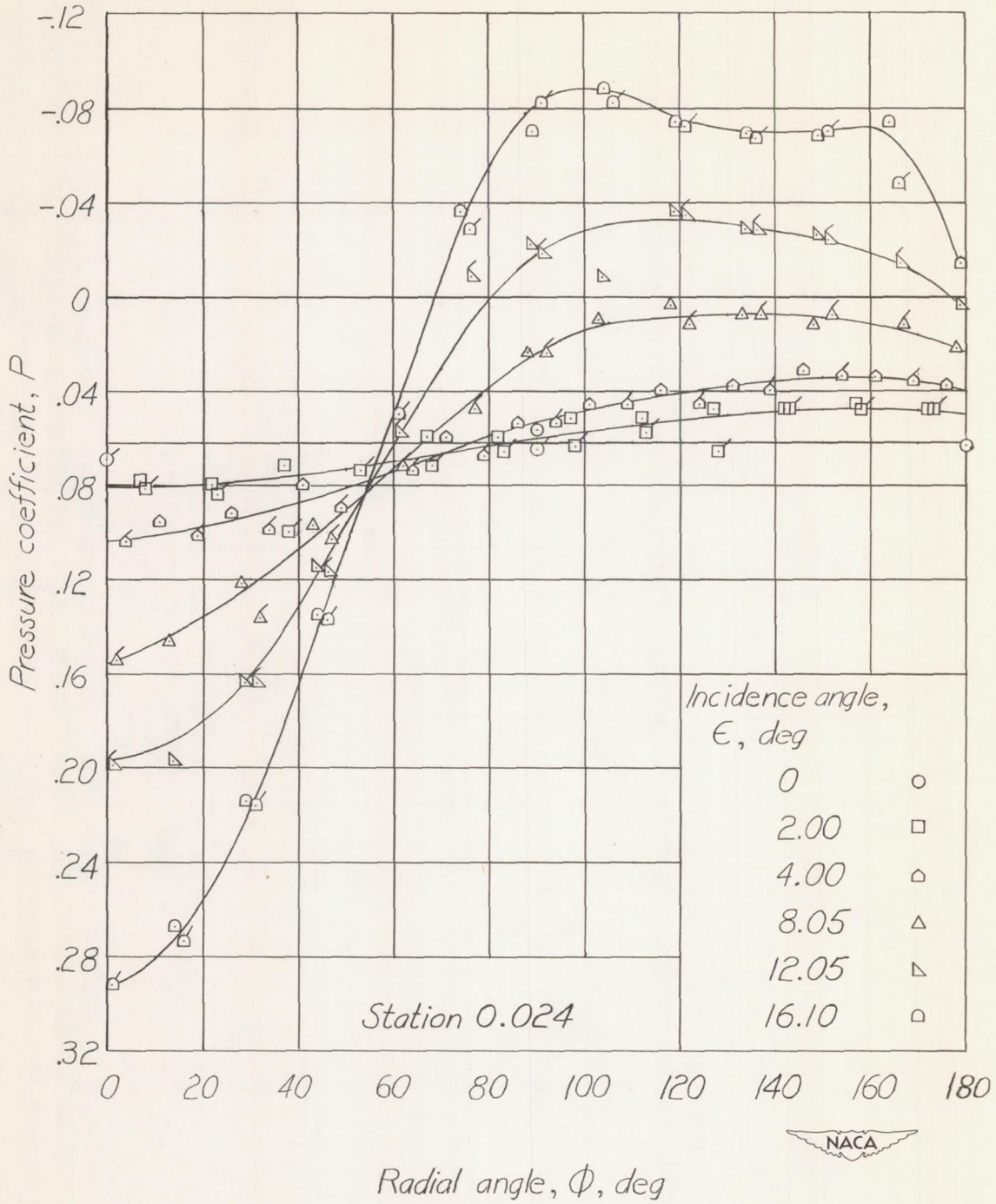


Figure 4.- Radial pressure distributions for representative incidence angles. (Flagged symbols indicate negative values of $\phi$.)

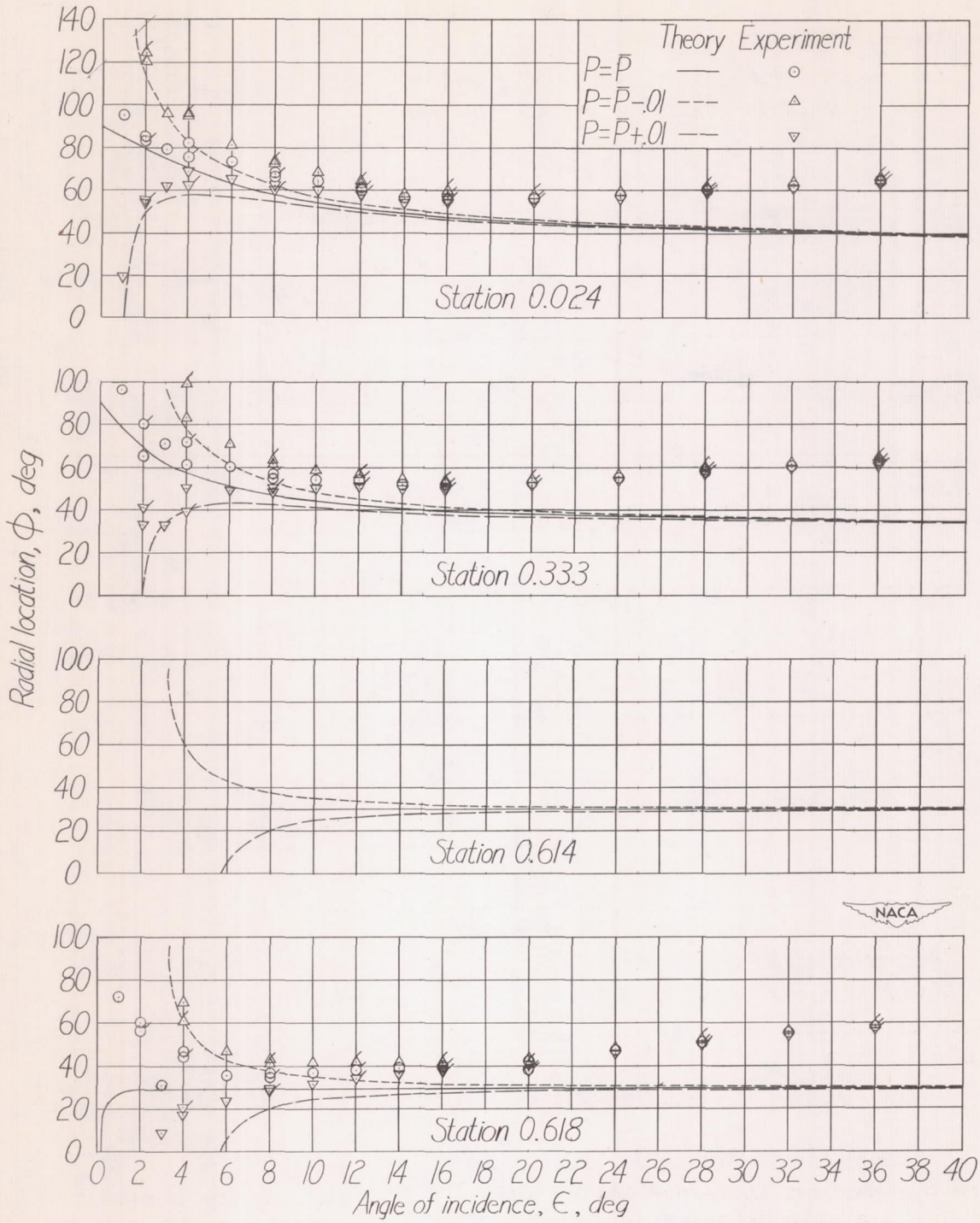


Figure 5.- Radial orifice locations for constant static pressure as a function of incidence angle for four representative stations along the body.

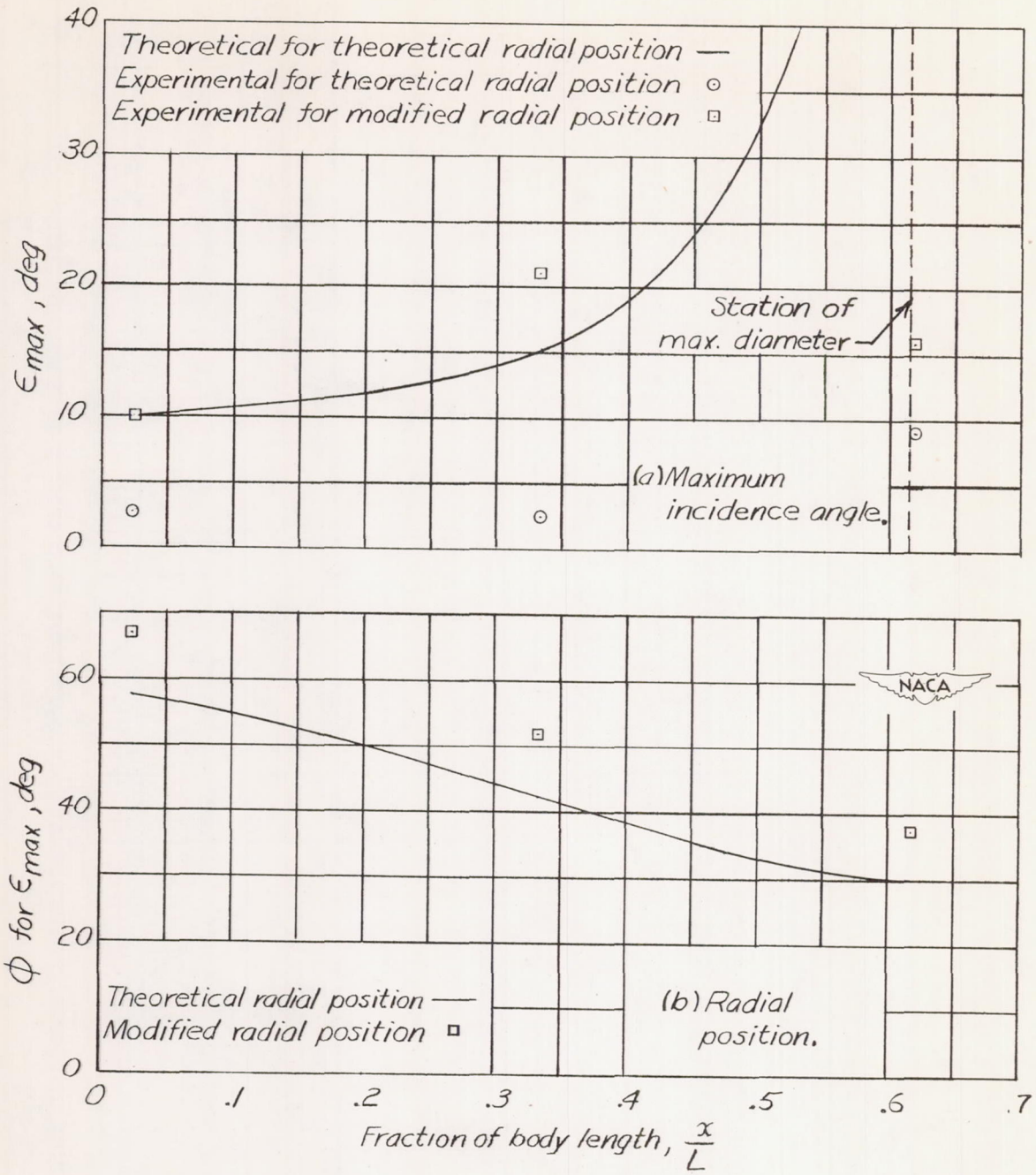


Figure 6.- Maximum incidence angles and orifice locations for constant static pressure as a function of body length.

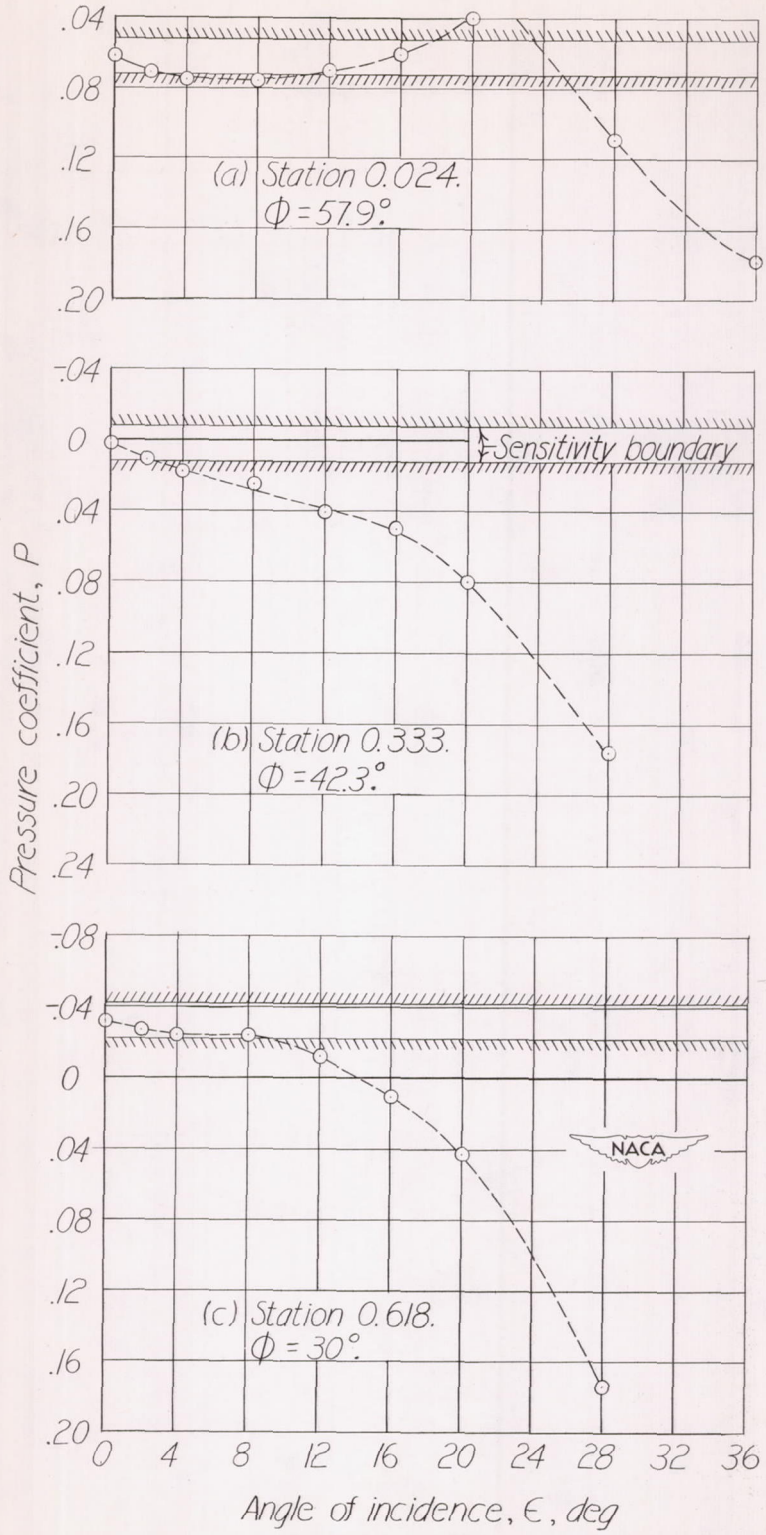


Figure 7.- Pressure coefficient as a function of angle of incidence for theoretical radial positions.

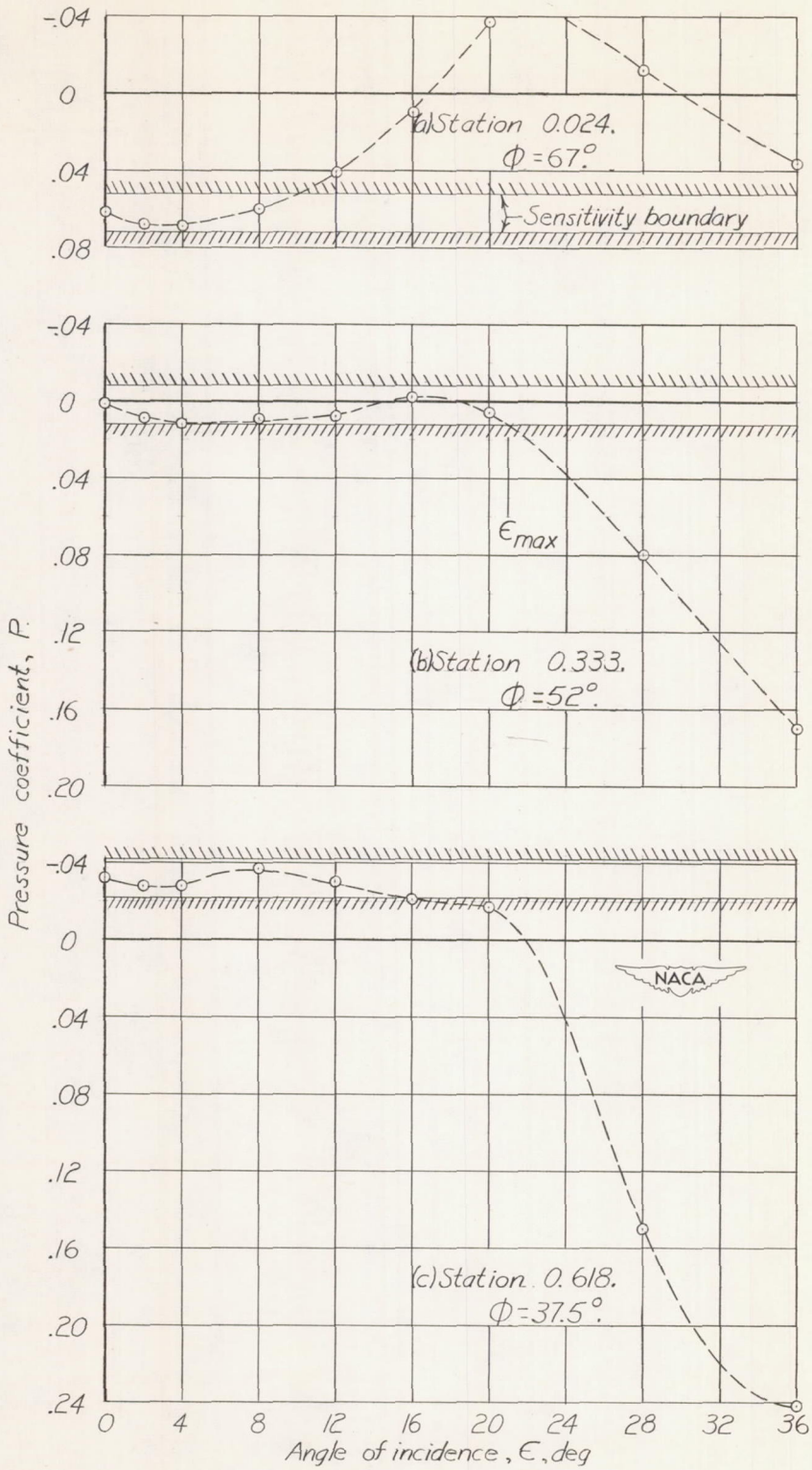


Figure 8.- Pressure coefficient as a function of angle of incidence for modified radial positions.

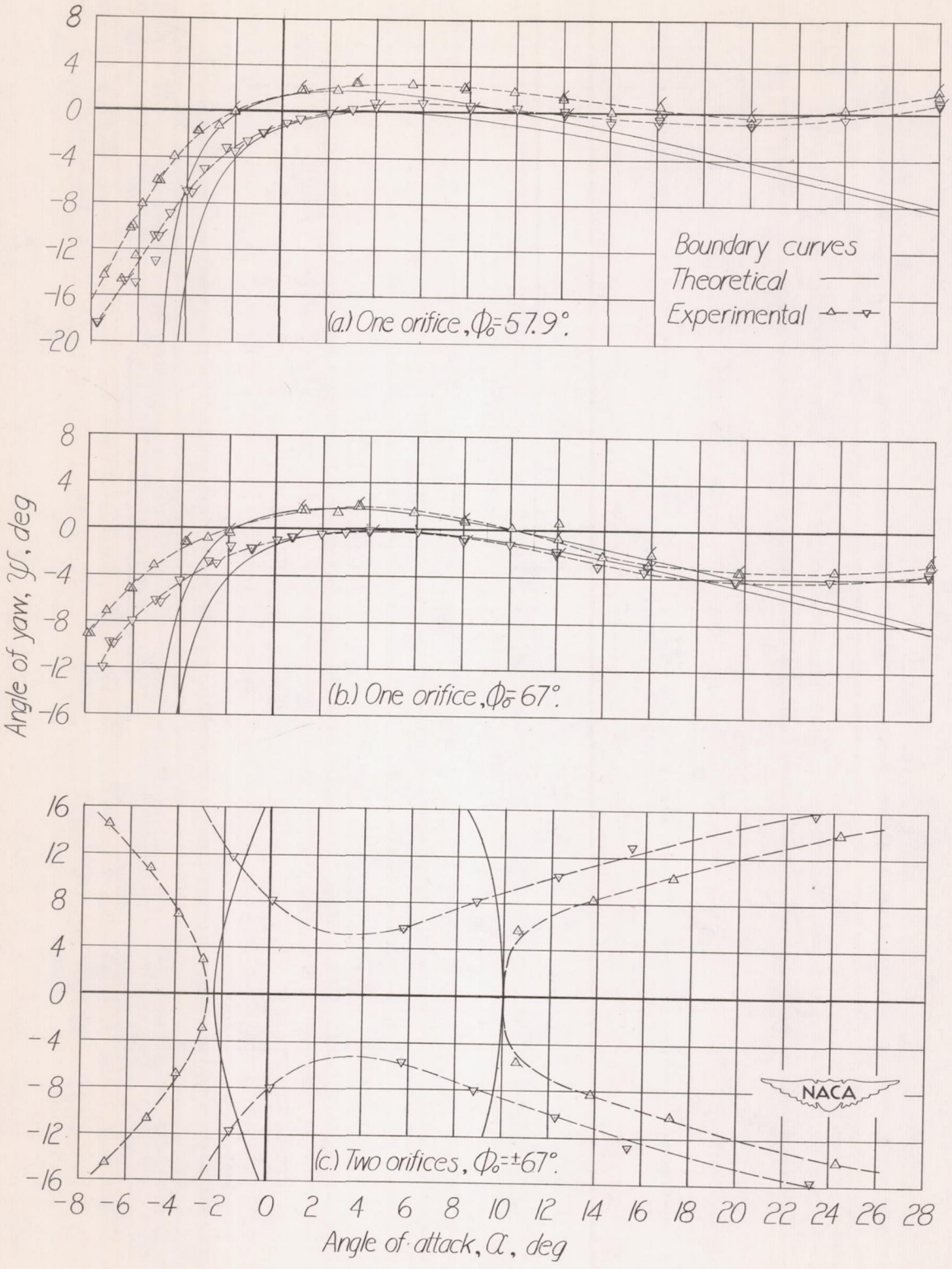


Figure 9.- Pitch-yaw boundary for station 0.024.

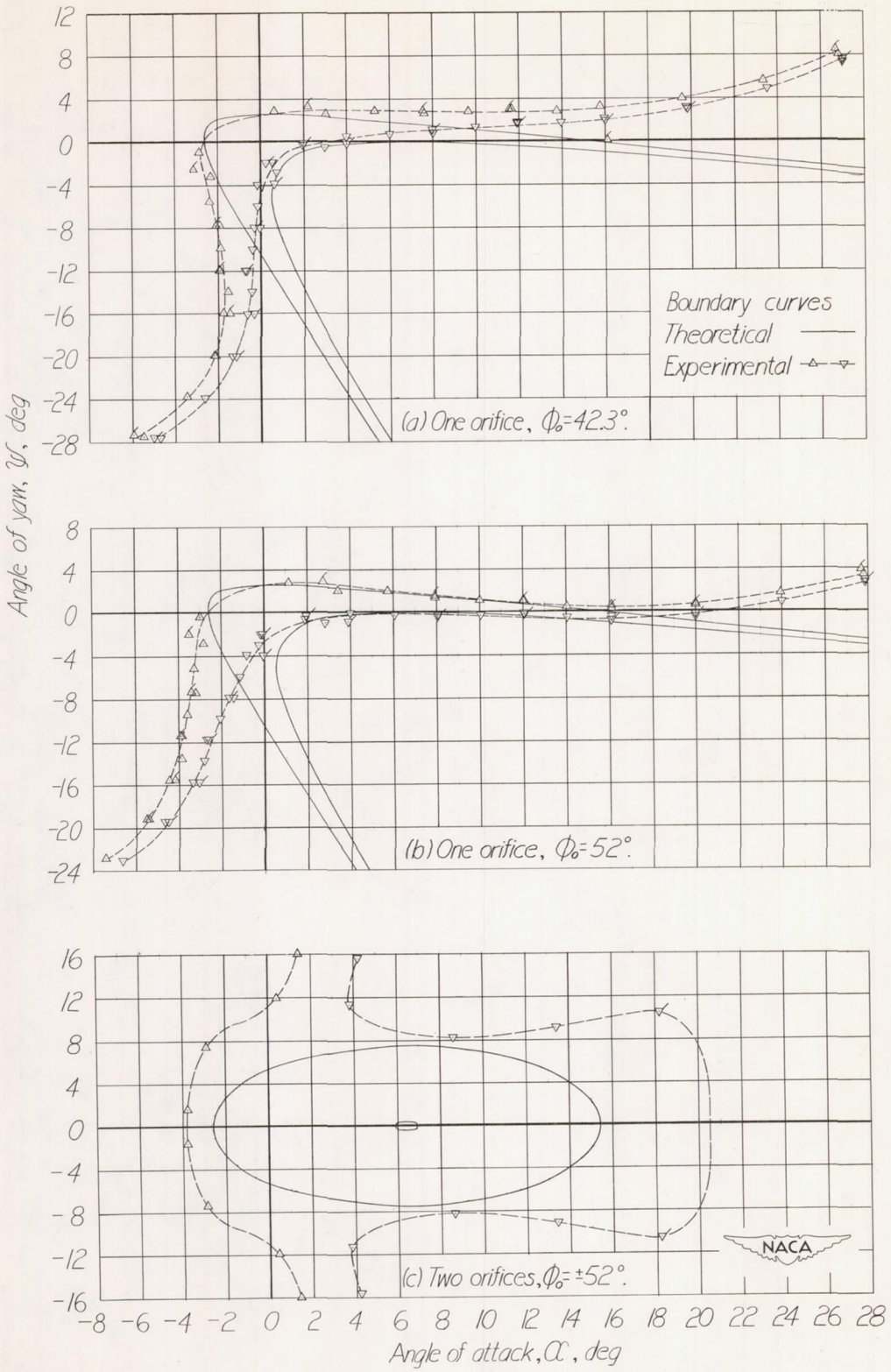


Figure 10.- Pitch-yaw boundary for station 0.333.

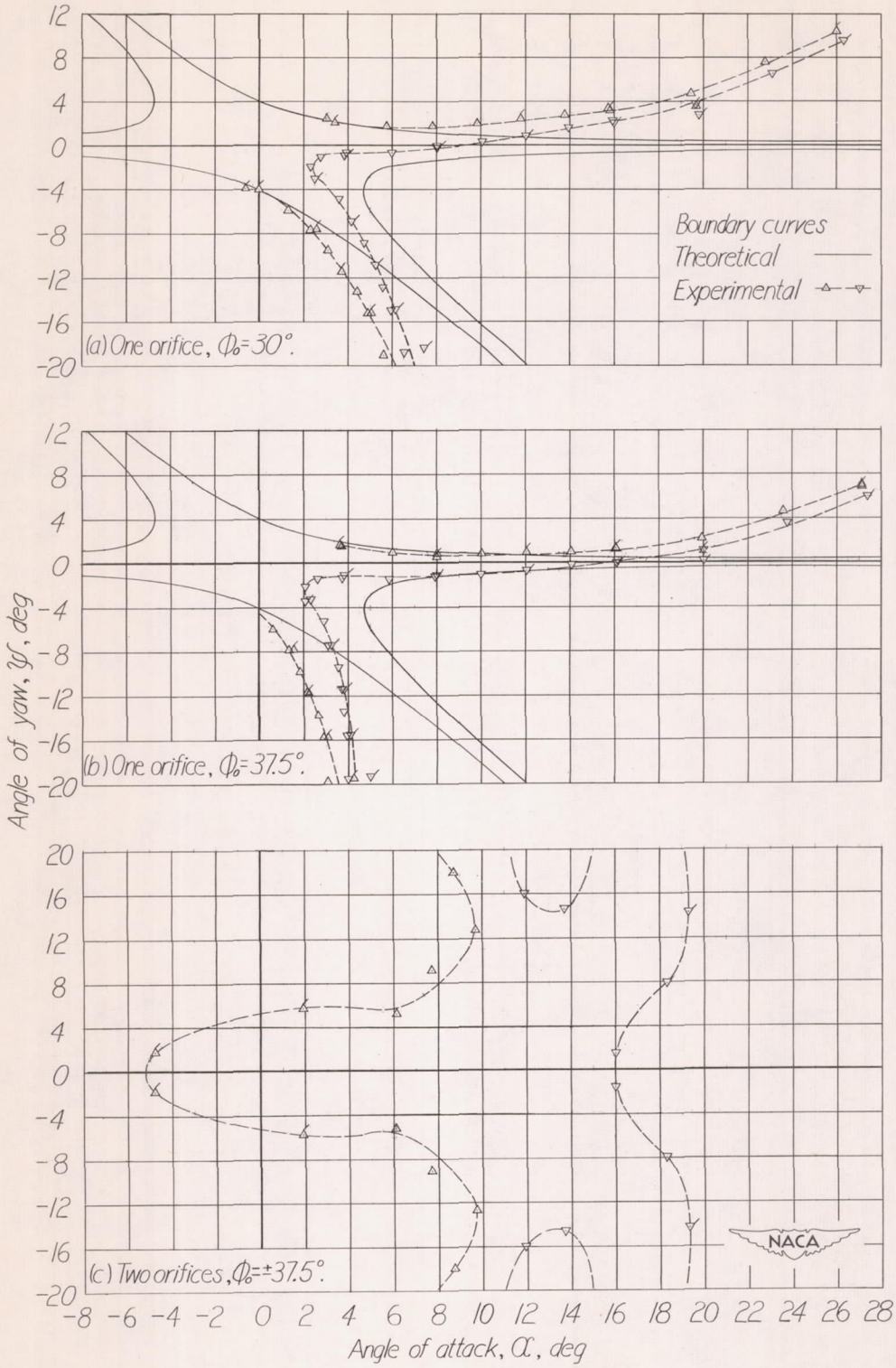


Figure 11.- Pitch-yaw boundary for station 0.618.

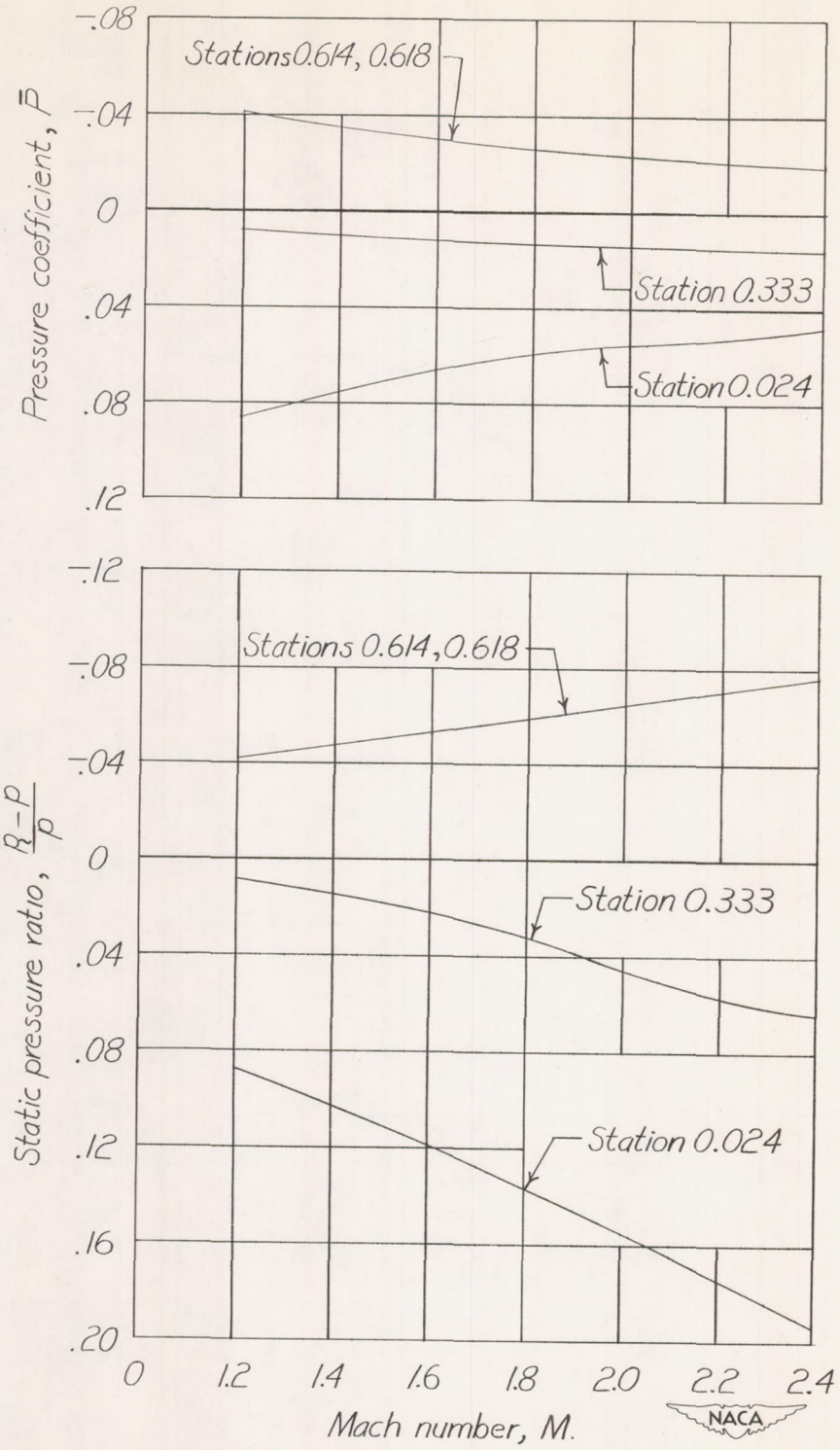


Figure 12.- Pressure coefficient and static pressure ratio for zero incidence as a function of Mach number for four representative stations.